Radiation tolerance studies of long wavelength infrared InAs/GaSb detectors

Alexander Soibel, Sir. B. Rafol, Arezou Khoshakhlagh, Jean Nguyen, Linda Hoglund, Anita Fisher, Sam. A. Keo, David Z.-Y. Ting and Sarath D. Gunapala

Jet Propulsion Laboratory, California Institute of Technology, 4800 Oak Grove Dr., Pasadena, CA, 91109, USA

Abstract

In this work we investigated the effect of proton irradiation on the performance of long wavelength infrared (LWIR) InAs/GaSb photodiodes (λ_c = 10.2μm) based on the complementary barrier infrared detector (CBIRD) design. We found that irradiation with 68MeV protons up to the total ionizing dose TID = 200 kRad results in only small (about 15%) decrease of the Quantum Efficiency and does not increase the operational bias of the photodiodes. However, the irradiation causes a significant increase of the dark current from j_d = 5x10^{-5} A/cm^2 at V_b = 0.1V and T = 80K to j_d = 6x10^{-3} A/cm^2 at TID = 200 kRad. This change in the dark current mechanism can be attributed to the onset of surface leakage current, generated by the trap assisted tunneling processes in the proton displacement damage areas near the device sidewalls.

Keywords: infrared detectors, long wavelength infrared (LWIR), InAs/GaSb photodiodes, complementary barrier infrared detector (CBIRD)

1. INTRODUCTION

Infrared (IR) detectors and Focal Plane Arrays (FPAs) are employed in numerous instruments developed by NASA for Earth and Planetary Science missions. Imagers used in space-based instruments are required to be radiation hard so as to exhibit only a minor performance degradation after exposure to ionizing radiation. The IR detectors most frequently used in space instrumentation are HgCdTe photodiodes; their radiation tolerance have been the subject of numerous studies.[1] Superlattice detectors based on InAs/GaSb/AlSb material layers[2] have demonstrated significant performance improvement in the last decade.[3] The InAs/GaSb superlattice is proven to have suppressed Auger generation-recombination rates[4,5] and low inter-band tunneling.[6,7] That in combination with complex heterodiodes designs enable realization of IR photodiodes with suppressed dark current.[8,9] The recent demonstration of N+-p complementary barrier infrared detector (CBIRD)[10,11] and subsequent design refinement has allowed to realize devices with zero turn-on bias, high quantum efficiency and dark current that only 2.5 times higher[12] than the dark current density estimated from Rule07,[13] commonly used for reference to the dark current of the best HgCdTe photodiodes. Preliminary study of their radiation tolerance have been conducted as they became valuable candidates for space-based instruments.[14,15,16,17]

In this work we investigated the effect of proton irradiation on the performance of long wavelength infrared (LWIR) InAs/GaSb photodiodes (λ_c = 10.2μm), based on complementary barrier infrared detector (CBIRD) design.[18] We found that irradiation with 68MeV protons up to the total ionizing dose, TID = 200kRad, results in only a small decrease in quantum efficiency (about 15%,) and no increase in operational bias of the photodiodes. However, the irradiation causes a significant increase in dark current, from j_d = 5x10^{-5} A/cm^2 at V_b = 0.1V and T=80K to to j_d = 6x10^{-4} A/cm^2 after the first

*Alexander.Soibel@jpl.nasa.gov; phone 818 393 0225; fax: 818 393 4540;
© 2016 California Institute of Technology. Government sponsorship acknowledged

irradiation with TID = 15kRad and to j_d = 6x10^{-3} A/cm^2 at TID = 200 kRad. This change in the dark current mechanism can be attributed to an onset of surface leakage current, which indicates that radiation damage near the device side walls has a major contribution to the dark current increase. Moreover, thermal-cycling of the device made only a minor improvement in the device performance, indicating there is proton displacement damage to the device structure. These results advance our understanding of mechanisms affecting performance of InAs/GaSb infrared photodiodes and can assist with development of radiation hard detectors for use in space-based instruments.

2. CBIRD DESIGN AND FABRICATION

Devices used in this work utilize the CBIRD design described in detail in Ref. 10. The active region of the structure consists of a 300-period (44 Å, 21 Å)-InAs/GaSb absorber SL sandwiched between an 80-period (46 Å, 12 Å)-InAs/AlSb hB SL on top, and a 60-period (22 Å, 21 Å)-InAs/GaSb eB SL on the bottom (Fig. 1). The active region is separated from the *p*-GaSb bottom contact by a 0.2 µm $InAs_{0.91}Sb_{0.09}$ layer. The hB SL and absorber SL are nominally doped at $n = 1\times10^{16}$ cm^{-3} and $p = 1\times10^{16}$ cm^{-3} respectively. The *p*-type eB SL is doped 2×10^{16} cm^{-3} at the top, then graded up to 1×10^{18} cm^{-3} on bottom. The *n*-InAsSb layer is doped 1×10^{18} cm^{-3} at the top, and graded up to 1×10^{19} cm^{-3} on bottom. The doping in the *p*-GaSb bottom contact is ramped down from 1×10^{19} cm^{-3} near the InAsSb side to 5×10^{17} cm^{-3}. The device structure was grown on a 50-mm-diameter Te-doped GaSb (100) substrate in a Veeco Applied-Epi Gen III molecular beam epitaxy (MBE) chamber, equipped with valve controlled cracking sources for group V: Sb_2 and As_2 fluxes. Following growth, wafers were characterized using X-ray diffraction, surface scan, AFM and low temperature photoluminescence (PL). The detector material was found to have lattice mismatch (-1389 ppm), low defect density (particle count from surface scan is 58.2 cm^{-2}) and high PL intensity, compared with the reference CBIRD wafer.[19]

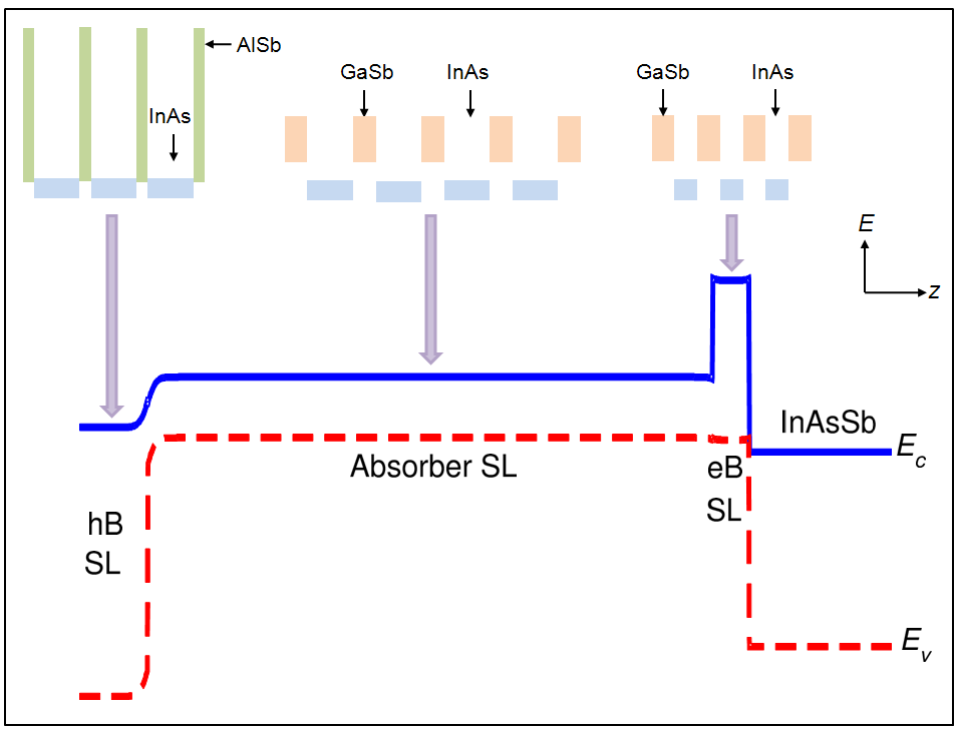

Figure 1. (Color online) Energy diagram of Complementary Barrier Infrared Detector (CBIRD)

Single pixel detectors were fabricated by dry etching using a combination of gases: $CH_4/H_2/BCl_3/Cl_2/Ar$ in an inductively coupled plasma (ICP) system.[20] Detectors were fully delineated, with etching into the bottom contact followed by Ohmic metal contact evaporation and a lift-off process. The detectors were mounted for back-side illumination and wire-bonded to ceramic leadless chip carrier (LCC).

3. TESTING METHODOLOGITY

Initially, detectors were fully characterized using a stationary set-up which includes dark current measurements at various operational temperatures and the photocurrent response measurements performed using a 1273K blackbody radiation source and a Nicolet Fourier Transform Infrared (FTIR) spectrometer. Later, detectors were loaded into IR Lab liquid nitrogen pour-fill dewar with a switchable cold shutter that enabled uninterrupted consecutive dark current and photocurrent measurements. The detectors were cooled down to 80K and tested with a moveable set-up that was later used during the radiation test. The detector characteristics obtained from the portable set-up were verified against the data collected from the stationary set-up. A minor difference between Quantum Efficiency (QE) measured by these two systems was taken into account by introducing an adjustment factor to correct QE measured by portable system. The 68MeV proton exposure was performed at the University of California, Davis, with isochronous cyclotron at Crocker Nuclear Laboratory. Detectors were kept unbiased at T = 80 K during irradiation and the time of each radiation session was set to about 15 min by adjusting the proton flux. The total ionizing dozes, TID, were 0, 15, 30, 50, 75, 100, 150 and 200 kRad, and the corresponding fluences were 1.4, 2.8, 4.8, 7.2, 9.6, 14.4 and 19.2 x10^{11} H+/cm^2. Dark current and photoresponse were tested prior to the irradiation and after each dose. After the full set of irradiations were completed, detectors were warmed to room temperature and kept at ambient conditions for several months. Then they were cooled down to T = 80K and re-tested with both portable and stationary systems.

4. SPECTRAL TEST

The measured external QE as a function of wavelength at T = 80 K and applied bias, V_b = 0.1V is shown in Figure 2a for back illuminated photodiodes without anti-reflection (AR) coating. The maximal QE, $QE_{max} \approx 0.35$ was measured at λ = 7μm and the device cut-off wavelength, λ_c = 10.2μm, was found from the inflection point. We used a narrow bandpass filter centered at λ_B = 8.6μm to measure the detector photoresponse during the irradiation studies. The QE at this wavelength, QE_B, vs TID is shown in Figure 2b. Before the irradiation $QE_B \approx 0.24$ and QE_B decreases with radiation dose to $QE_B \approx 0.21$ at TID = 200 kRad. The QE decrease is small, less than 15% over the full range of TID. The detector thermocycling resulted only in a very minor increase of Quantum Efficiency to $QE_B \approx 0.22$.

From transmission measurements the superlattice absorption coefficient (α) was estimated to $\alpha \sim 2500\text{cm}^{-1}$ at λ = 7 μm and the substrate transmission is found to be close to 100% at this wavelength (not shown). Assuming full reflection of the light at the top metal contact, we can estimate the minority carriers (electrons) diffusion length, L_e, from the absorption coefficient and QE value.[21] The estimated diffusion length $L_e \approx$ 5-6 μm is significantly longer than the absorber thickness d = 2 μm. In this regime, when diffusion length is longer than the absorber thickness, the decrease of the diffusion length with TID would only result in a small degradation of QE.

The decrease of the minority carrier lifetime with TID has not been yet measured for InAs/GaSb superlattice. A small change of QE with TID observed in these devices may indicate that only minor decrease of the lifetime occurs. Indeed, the minority carrier lifetime in LWIR InAs/GaSb superlattice is relatively short, $\tau \approx$ 30 ns,[22] due to the non-radiative recombination through defects states associated with Ga atoms[23] and potentially assisted by multiphonon processes.[22] The defects are intrinsically present in the superlattice and can continue to dominate the recombination process even after exposure to the radiation.

Figure 2c shows the bias dependence of Quantum Efficiency at various TID. These CBIRD photodiodes can operate at zero applied bias and radiation does not change the operational bias. The radiation hardness of diode operational bias is a favorable property of our CBIRD design.

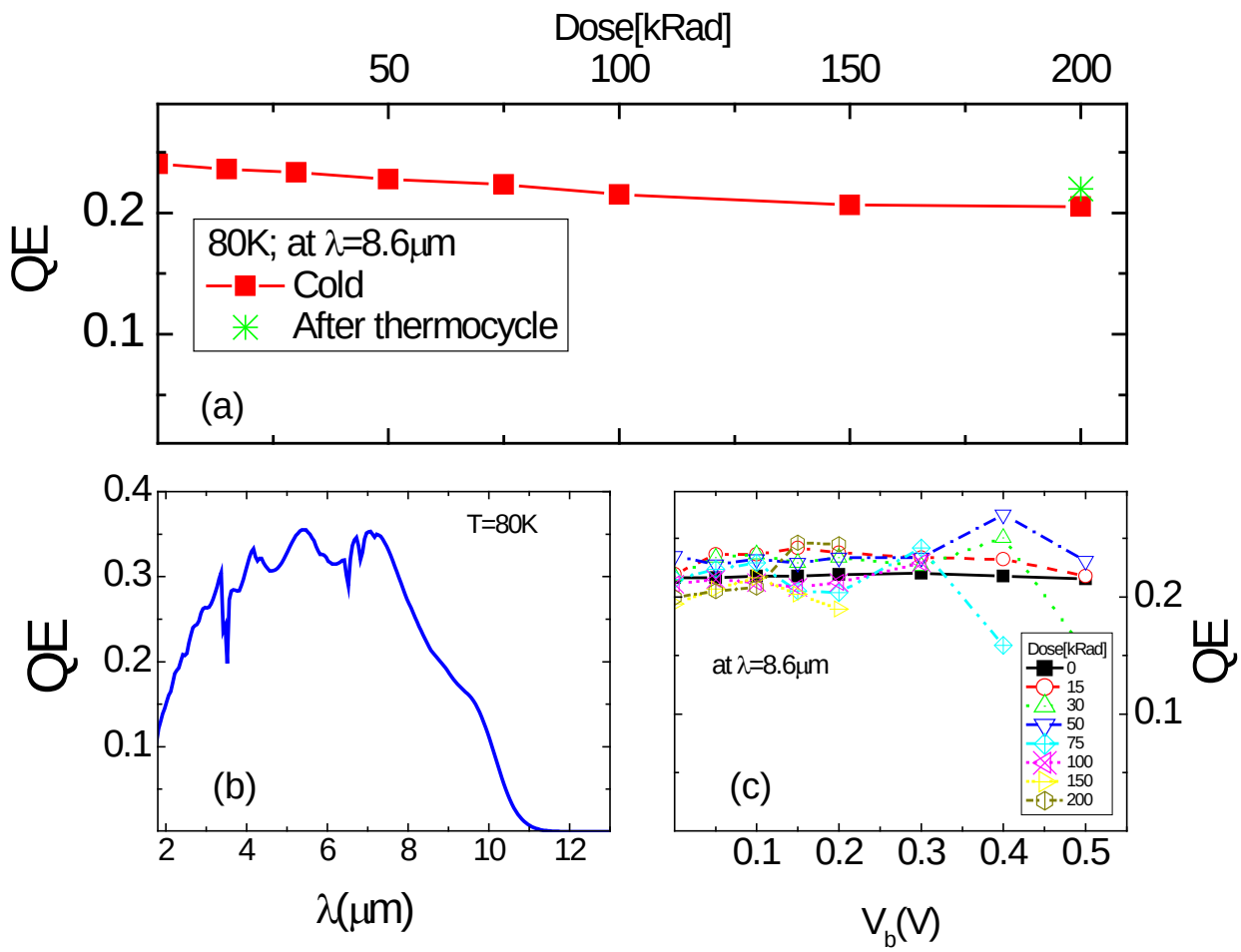

Figure 2. (Color online) (a) External Quantum Efficiency measured at T = 80K for backside illumination and V_b = -0.1V. (b) Quantum Efficiency measured at λ = 8.6μm vs. irradiation dose. Quantum Efficiency measured after thermocyling is also shown. (c) Quantum Efficiency vs. applied bias for the total different irradiation doses as indicated in the graph.

5. SPECTRAL TEST

Figure 3a shows the dark current density of 150μm square photodiode (device A) operating at T =80K for various TIDs. Dark current density of these devices increases with TID and the shape of $j(V)$ curves exhibits a pronounced change just after the first irradiation. The dark current density is j_d = 5x10^{-5} A/cm^2 at V_b = 0.1V at TID = 0 kRad and it increases by order of magnitude to j_d = 6x10^{-4} A/cm^2 after the first irradiation with TID = 15 kRad. The dark current continues to increase linearly with TID (Fig. 3b) reaching j_d = 6x10^{-3} A/cm^2 at TID = 200 kRad. The change in the dark current with dose can be described, as $j_d = j_{d0}+K_{jd}\Phi p$, where K_{jd} is the dark damage factor and Φp is the proton irradiation fluence. Fit to data shown in Figure 2c gives $K_{jd}\approx$ 2.2-3.5x10^{-15} (A/cm^2) /(H+/cm^2). Detector thermocycling resulted only in a small reduction of dark current to j_d = 4x10^{-3} A/cm^2 (Fig 3a and 3b), showing that the radiation damage is not annealed at room temperature and can be attributed to the displacement effects.

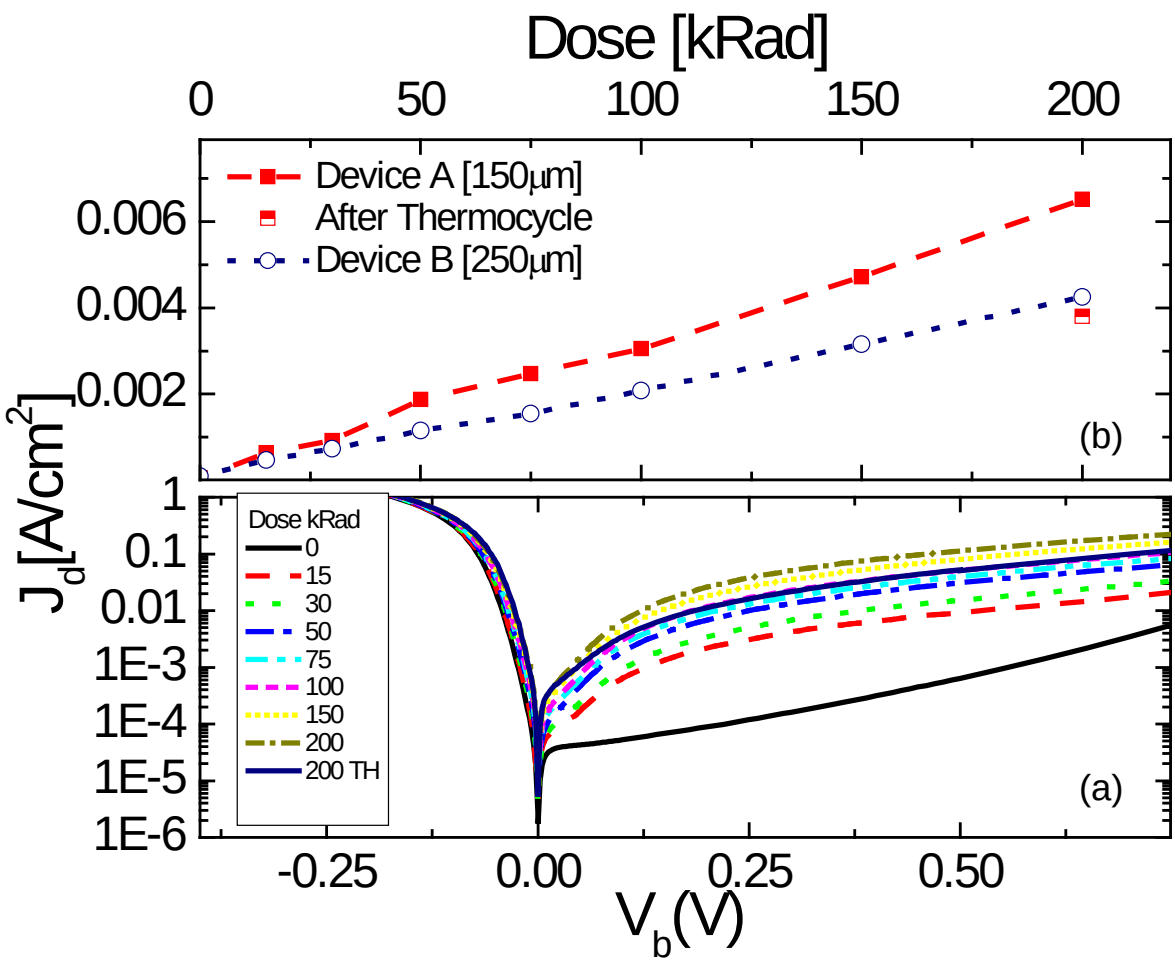

Figure 3. (Color online) (a). Dark current density of 150μm square single pixel photodiode (Device A) operating at temperature T = 80K measured after the detector exposure to proton irradiation with total irradiation dose (TID) shown in the graph legend. The dark current measured after thermocycling is denoted as "200TH". (b) Dark current density of 150μm (device A) and 250μm (device B) measured at T=80K and V_b = 0.1V vs. TID. Dark current density after thermocycling is also shown in the graph.

Figure 4 shows the dark current density of square 125, 150 and 250 μm photodiodes vs. perimeter/area ratio, P/A. Before the irradiation, there is no clear dark current dependence on the perimeter/area ratio and the two large devices have the largest dark current in this set. The situation changes after the irradiation when a linear dependence of the dark current on the perimeter/area is observed. We can extract the bulk dark current after the irradiation, j_{ba}, from the intersection of the linear fit curve with the axis. This gives $j_{ba} \approx 2\text{x}10^{-3}$ A/cm^2 which is significantly lower than the dark current measured for 150μm device after irradiation, $j \approx 6\text{x}10^{-3}$ A/cm^2 but is still much higher than the photodiode dark current before the irradiation, $j_d = 5\text{x}10^{-5}$ A/cm^2. This indicates that the irradiation increases both bulk and surface dark currents, but the damage near the detector side wall has a larger effect on the dark current.

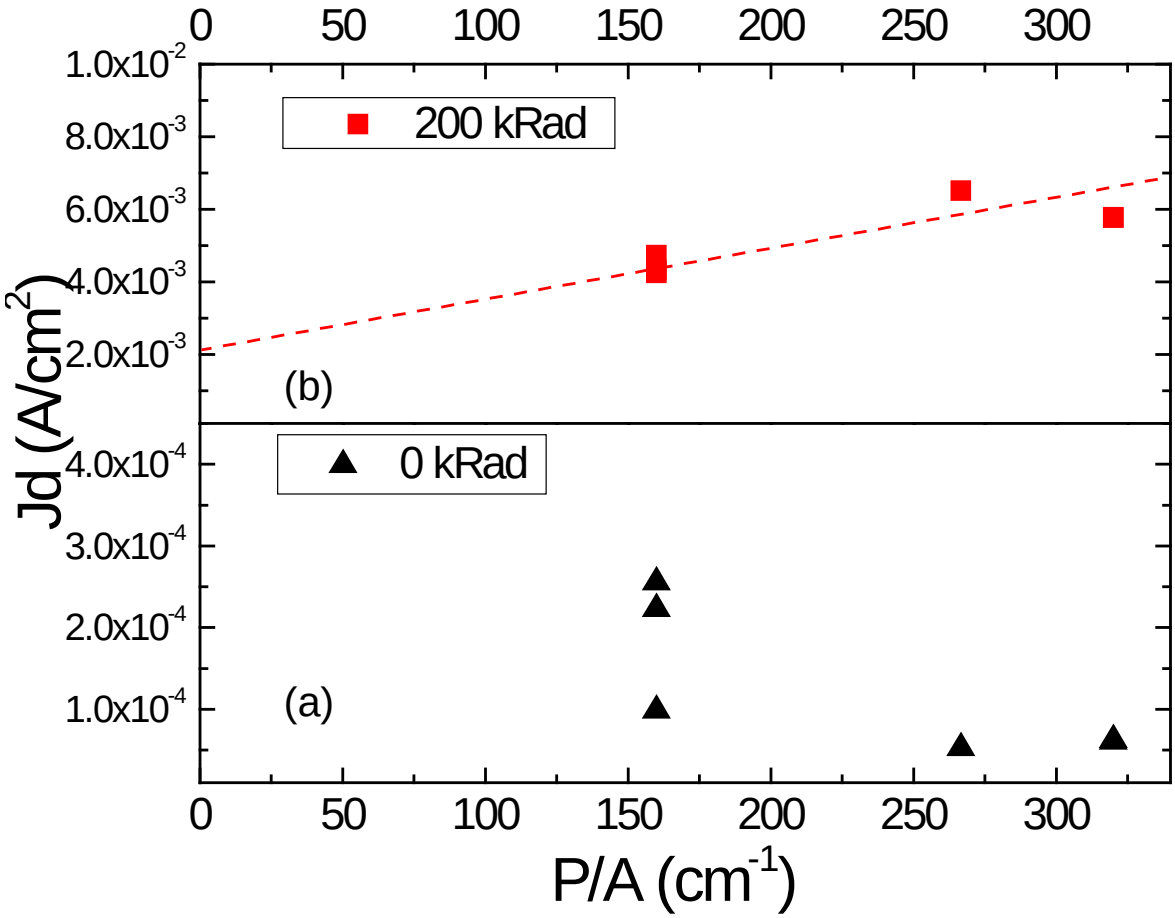

Figure 4. (Color online) Dark current density measured at T = 80K and V_b = 0.1V vs. perimeter-to-area (P/A) ratio for TID = 0 kRad (panel a) and 200kRad (panel b). Red dashed line is a linear fit to data collected at TID=200kRad.

6. DISCUSSION

In summary, we found that proton irradiation up to the total ionization dose 200kRad has only a minor effect on the spectral characteristics of LWIR InAs/GaSb superlattice photodiodes based on CBIRD design. At the same time, proton irradiation significantly increases dark current measured in these devices. This change in the dark current mechanism is attributed to the onset of the surface leakage current. It indicates that material damage close to the detector side walls increases the surface leakage current, which has a major contribution to the device degradation. Adequate passivation of the detector side wall or development of planar device geometry can potentially reduce the radiation damage and enable radiation hard InAs/GaSb superlattice detectors.

7. ACKNOWLEDGEMENTS

The research described in this publication was carried out at the Jet Propulsion Laboratory, California Institute of Technology, under a contract with the National Aeronautics and Space Administration

REFERENCES

[1]. Pickel, J., Kalma, A., Hopkinson, G., and Marshall, C., “Radiation effects on photonic imagers - A historical perspective”, IEEE Transactions on Nuclear Science 50 (3), 671-688 (2003).

[2]. G. Saihalasz, G., Tsu, R., and Esaki, L., “New semiconductor superlattice”, Applied Physics Letters 30 (12), 651-653 (1977).

[3]. Ting, D., Soibel, A., Hoglund, L., Nguyen, J., Hill, C., Khoshakhlagh, A., Gunapala, S., Rhiger, D., and Jagadish, C., “Type-II Superlattice Infrared Detectors”, Advances in Infrared Photodetectors 84, 1-57 (2011).

[4].Grein, C., Young, P., and Ehrenreich, H., “Minority carrier lifetimes in ideal InGaSb/InAs superlattice”, Applied Physics Letters 61 (24), 2905-2907 (1992).

[5]. Youngdale, E., Meyer, J., Hoffman, C., Bartoli, F., Grein, C., Young, P., Ehrenreich, H., Miles, R., and Chow, D., “ Auger lifetime enhancement in InAs-GaInSb superlattice”, Applied Physics Letters 64 (23), 3160-3162 (1994).

[6]. Smith, D., McGill, T., and Schulman, J., “Advantages of the HgTe-CdTe superlatticee as infrared detector”, Applied Physics Letters 43 (2), 180-182 (1983).

[7]. Mailhiot, C., McGill, T., and Schulman, J, “Tunneling and propagating transport in GaAs-GaAlAs-GaAs(100) double heterojunctions”, Journal of Vacuum Science & Technology B 1 (2), 439-444 (1983).

[8]. Fuchs, F., Weimer, U., Pletschen, W., Schmitz, J., Ahlswede, E., Walther, M., Wagner, J., and Koidl, P., “High performance InAs/Ga1-xInxSb superlattice infrared photodiodes”, Applied Physics Letters 71 (22), 3251-3253 (1997).

[9]. Vurgaftman, I., Aifer, E., Canedy, C., Tischler, J., Meyer, J., Warner, J., Jackson, E., Hildebrandt, G., and Sullivan, G., “Graded band gap for dark-current suppression in long-wave infrared W-structured type-II superlattice photodiodes”, Applied Physics Letters 89 (12) (2006).

[10]. Ting, D., Hill, C., Soibel, A., Keo, S., Mumolo, S., Nguyen, J., and Gunapala, G., “A high-performance long wavelength superlattice complementary barrier infrared detector”, Applied Physics Letters 95 (2) (2009).

[11]**.** Ting, D., Soibel, A., Khoshakhlagh, A., Nguyen, J., Höglund, L., Keo, S., Mumolo, J., and Gunapala, S., “ *Appl. Phy. Lett.* **102**(12), 121109 (2013).

[12]. Soibel, A., Rafol, S., Khoshakhlagh, A., Nguyen, J., Hoeglund, L., Keo, S., Mumolo, J., Liu, J., Liao, A., Ting, D., and Gunapala, S., “Long Wavelength Infrared Superlattice Detectors and FPAs Based on CBIRD Design”, IEEE Photonics Technology Letters 25 (9), 875-878 (2013).

[13]. Tennant, W., “ "Rule 07" Revisited: Still a Good Heuristic Predictor of p/n HgCdTe Photodiode Performance?”, Journal of Electronic Materials 39 (7), 1030-1035 (2010).

[14]. Weaver, B., and Aifer, E., “Radiation Effects in Type-Two Antimonide Superlattice Infrared Detectors”, IEEE Transactions on Nuclear Science 56 (6), 3307-3309 (2009).

[15]. Jackson, E., Aifer, E., Canedy, C., Nolde, J., Cress, C., Weaver, B., Vurgaftman, I., Warner, J., Meyer, J., Tischler, J., Shaw, S., and Dedianous, C., “ Radiation Damage in Type II Superlattice Infrared Detectors”, Journal of Electronic Materials 39 (7), 852-856 (2010).

[16]. Cowan, V., Morath, C., Hubbs, J., Myers, S., Plis, E., and Krishna, S., “Radiation tolerance characterization of dual band InAs/GaSb type-II strain-layer superlattice pBp detectors using 63 MeV protons”, Applied Physics Letters 101 (25) (2012).

[17]. Morath, C., Cowan, V., Treider, L., Jenkins G., and Hubbs, J., "Proton Irradiation Effects on the Performance of III-V-Based, Unipolar Barrier Infrared Detectors", IEEE Transactions on Nuclear Science 62 (2), 512-519 (2015).

[18] Soibel, A., Rafol, S., Khoshakhlagh, Nguyen, J., Hoglund, L., Fisher, A., Keo, S., Ting, D., and Gunapala, S., "Proton radiation effect on performance of InAs/GaSb complementary barrier infrared detector", Appl. Phys. Lett. 107, 261102 (2015).

[19]. Khoshakhlagh, A., Ting, D., Soibel, A., Hoglund, L., Nguyen, J., Keo, S., Liao, A., and Gunapala, S., "Growth and characteristics of type-II InAs/GaSb superlattice-based detectors ", *Proc. SPIE*, vol. 8154, 81540K-0 - 81540K-6 (2011).

[20]. Nguyen, J., Soibel, A., Ting, D., Hill, C., Lee, M., and Gunapala, S., "Dark current analysis of InAs/GaSb superlattices at low temperatures", Applied Physics Letters **97**(5), 051108 (2010).

[21]. Djuric, Z., and Jaksic, Z., "Back side reflection influence on Quantum Efficiency of photovoltaic devices', Electronics Letters 24 (17), 1100-1101 (1988).

[22]. Donetsky, D., Belenky, G., Svensson, S., and Suchalkin, S., "Minority carrier lifetime in type-2 InAs-GaSb strained-layer superlattices and bulk HgCdTe materials", Applied Physics Letters 97 (5) (2010).

[23]. Steenbergen, E., Connelly, B., Metcalfe, G., Shen, H., Wraback, M., Lubyshev, D., Qiu, Y., Fastenau, J., Liu, A., Elhamri, S., Cellek, O., and Zhang, Y., "Significantly improved minority carrier lifetime observed in a long-wavelength infrared III-V type-II superlattice comprised of InAs/InAsSb", Applied Physics Letters 99 (25) (2011).